Soft gluon radiation in hadronic $t\bar{t}$ production

V. A. Khoze and J. Ohnemus
Department of Physics, University of Durham, Durham, DH1 3LE, England

W. J. Stirling
Departments of Mathematical Sciences and Physics, University of Durham, Durham, DH1 3LE, England
(Received 24 August 1993)

We investigate soft gluon radiation in hadronic $t\bar{t}$ production. By taking the top quark decay properly into account, we are able to study the interplay of radiation both before and after the decay of the top quarks. The production-decay and decay-decay radiative interferences depend sensitively on the relative size of the gluon energy and the decay width. Radiation patterns for various production mechanisms are compared.

PACS number(s): 12.38.Bx, 14.65.Ha, 14.70.Dj

I. INTRODUCTION

Discovery of the top quark—one of the basic components of the standard model—is one of the most important goals of present and future high-energy colliders. At present, indirect evidence from electroweak radiative corrections suggests a top quark mass between 100 and 200 GeV (see for example Ref. [1]), and null results from searches at the Fermilab $p\bar{p}$ collider yield a 95% C.L. lower limit of 108 GeV and 103 GeV from the Collider Detector at Fermilab CDF [2] and D0 [3] collaborations, respectively. Optimistically, the top quark will be discovered at the Fermilab $p\bar{p}$ collider in the next few years.

The two most important properties of the top quark, which can be measured once its existence is established, are the mass m_t and the decay width Γ_t. The first of these is a fundamental parameter of the theory, while the second provides an opportunity to check the existence of any non–standard-model decay channels. However, obtaining precise measurements of these parameters at a hadron collider is a far from easy task. In particular, a detailed knowledge of the structure of the final state is necessary. For example, gluon radiation from the initial state, from the produced top quarks, and from the top quark decay products can influence the reconstruction of the top mass from its decay products. Soft gluon radiation, in particular the interference between radiation before and after top decay, also depends sensitively on the decay width [4,5].

In this paper we study the "antenna pattern" of soft gluon radiation in $t\bar{t}$ production in high-energy hadron-hadron collisions. In particular, we are interested in (a) the process dependence ($q\bar{q} \to t\bar{t}$ vs $gg \to t\bar{t}$) of this radiation and (b) the effect of the top quark instability on the radiation pattern. The former depends on the color topology of the different processes, while the latter induces dependence on Γ_t and on the orientation of the top decay products. Our study builds on earlier work. In Ref. [4], for example, the color-singlet production process $e^+e^- \to t\bar{t} \to bW^+\bar{b}W^-$ was analyzed in detail, and a gauge-invariant approach for identifying and calculating the various production and decay contributions to the radiation pattern was presented. It is the extension of these ideas to the more complicated processes $q\bar{q}, gg \to t\bar{t} \to bW^+\bar{b}W^-$ which constitutes the main goal of the present study. The radiation pattern for *stable* top production $q\bar{q}, gg \to t\bar{t}$ has been analyzed in detail in Refs. [6,7] (see also [8]). Again, our purpose here is to extend this analysis to the experimentally more relevant $bW^+\bar{b}W^-$ final state. Note that in our analysis the soft gluons are sufficiently energetic so that a perturbative treatment is valid. Nonperturbative effects, including possible long distance interactions with the spectator partons, have been discussed in Ref. [9].

Our aim, then, is to give a complete and systematic account of soft gluon radiation in hadronic $t\bar{t}$ production, accounting for color topology of the different processes, decay product kinematics, and finite top width effects. In the next section, we describe a method for writing down the antenna pattern for *any* $t\bar{t}$ production process of the form $AB \to t\bar{t} \to bW^+\bar{b}W^-$. Although our main interest here is in the strong interaction processes $q\bar{q}, gg \to t\bar{t}$, we also present results for $q\bar{q} \to Z^* \to t\bar{t}$ and $gg \to H \to t\bar{t}$. These processes, with their unique color structure, are useful for comparison. In Sec. III we present some numerical results. In particular, we consider final states with particular (and experimentally typical) orientations of the final state b quarks and W bosons. We study the soft gluon antenna patterns, focusing on the process and top width dependence. Our objective is not to emulate a Monte Carlo analysis including realistic detector acceptances, but rather to emphasize the most important features of the soft gluon radiation accompanying $t\bar{t}$ production and decay which should be taken into account in more realistic studies. Finally, in Sec. IV we summarize our main results.

II. FORMALISM

In the soft gluon limit, the radiation pattern for *any* elementary $2 \to 2$ hard scattering process f can be written as [8]

$$\overline{\sum}|\mathcal{M}^{(f)}|^2 = \sum_{ij} \widehat{ij}\, A_{ij}^{(f)} , \tag{1}$$

where the sum i,j is over the external particles. The "antenna" $\widehat{ij}$ is defined by

$$\widehat{ij} \equiv \frac{p_i \cdot p_j}{p_i \cdot k\; p_j \cdot k} , \tag{2}$$

where p_i and p_j are the four-momentum vectors of particles i and j and k is the gluon four-momentum vector. The coefficients $A_{ij}^{(f)}$ are functions of the kinematic invariants of the $2 \to 2$ process. The simplest example is the process $e^+e^- \to q\bar{q}(g)$ where, for massless quarks, there is only one such antenna and $\overline{\sum}|\mathcal{M}|^2 \propto \widehat{q\bar{q}}$.

In the present context we are interested in the following $t\bar{t}$ production processes:

$$e^-e^+ \to t\bar{t} , \tag{3a}$$
$$q\bar{q} \to Z^* \to t\bar{t} , \tag{3b}$$
$$gg \to H \to t\bar{t} , \tag{3c}$$
$$q\bar{q} \to t\bar{t} , \tag{3d}$$
$$gg \to t\bar{t} . \tag{3e}$$

(Note that the soft gluon radiation pattern for the process $\gamma\gamma \to t\bar{t}$ is identical to the pattern for the $e^-e^+ \to t\bar{t}$ process.) Labeling the initial and final state momenta by

$$\begin{aligned} A(k_1) + B(k_2) &\to t(q_1) + \bar{t}(q_2) \\ &\to b(p_1) + W^+ + \bar{b}(p_2) + W^- , \end{aligned} \tag{4}$$

the general form of the differential distribution for soft gluon radiation (k^μ) is [4]

$$\frac{1}{d\sigma_0}\,\frac{d\sigma}{d\omega_g\, d\cos\theta_g\, d\phi_g} = \frac{\alpha_s}{4\pi^2}\,\omega_g\,\mathcal{F} , \tag{5}$$

where $d\sigma_0$ is the differential cross section for the lowest-order process (i.e., with no gluon radiation), ω_g is the energy of the soft gluon, and α_s is the strong coupling. For the case of *stable* top quarks and massless initial state particles, the distribution function $\mathcal{F}$ has the general form

$$\begin{aligned} \mathcal{F}_0 = {} & c_1\widehat{k_1k_2} + c_2\widehat{k_1q_1} + c_3\widehat{k_1q_2} + c_4\widehat{k_2q_1} + c_5\widehat{k_2q_2} \\ & + c_6\widehat{q_1q_2} + c_7\widehat{q_1q_1} + c_8\widehat{q_2q_2} , \end{aligned} \tag{6}$$

where the antennae are defined as before by

$$\widehat{pq} \equiv \frac{p \cdot q}{p \cdot k\; q \cdot k} . \tag{7}$$

The coefficients c_i are given in Table I for the five $t\bar{t}$ production processes listed in Eq. (3). The functions X and Y appearing in the $gg \to t\bar{t}$ process are discussed later.

The general method for treating *unstable* heavy particles such as the top quark has been presented in Ref. [4]. The top quark *decay* is included by letting $\mathcal{F}_0 \to \mathcal{F}$, with $\mathcal{F}$ given by Eq. (6) with the replacements

$$\begin{aligned} \widehat{k_1k_2} &\to \widehat{k_1k_2} , \\ \widehat{k_1q_1} &\to \widehat{k_1q_1} + \chi_1\,[\widehat{k_1p_1} - \widehat{k_1q_1}] , \\ \widehat{k_1q_2} &\to \widehat{k_1q_2} + \chi_2\,[\widehat{k_1p_2} - \widehat{k_1q_2}] , \\ \widehat{k_2q_1} &\to \widehat{k_2q_1} + \chi_1\,[\widehat{k_2p_1} - \widehat{k_2q_1}] , \\ \widehat{k_2q_2} &\to \widehat{k_2q_2} + \chi_2\,[\widehat{k_2p_2} - \widehat{k_2q_2}] , \\ \widehat{q_1q_2} &\to \widehat{q_1q_2} + \chi_2\,[\widehat{q_1p_2} - \widehat{q_1q_2}] + \chi_1\,[\widehat{q_2p_1} - \widehat{q_1q_2}] \\ &\quad + \chi_{12}\,[\widehat{p_1p_2} - \widehat{q_1p_2} - \widehat{q_2p_1} + \widehat{q_1q_2}] , \\ \widehat{q_1q_1} &\to 2\widehat{q_1q_1} + \widehat{p_1p_1} - 2\widehat{q_1p_1} + 2\chi_1\,[\widehat{q_1p_1} - \widehat{q_1q_1}] , \\ \widehat{q_2q_2} &\to 2\widehat{q_2q_2} + \widehat{p_2p_2} - 2\widehat{q_2p_2} + 2\chi_2\,[\widehat{q_2p_2} - \widehat{q_2q_2}] . \end{aligned} \tag{8}$$

We make the following comments concerning the above results.

(i) For unstable top quarks, we see that there are additional contributions from antennae involving the daughter b quarks, corresponding to gluon emission both before *and* after the t quarks decay. The profile functions χ, which depend on the top width Γ_t and determine the size of the interference effects, are given by [4]

$$\chi_i = \frac{m_t^2\Gamma_t^2}{(q_i \cdot k)^2 + m_t^2\Gamma_t^2} , \tag{9}$$

$$\chi_{12} = \frac{m_t^2\Gamma_t^2\;(q_1 \cdot k\; q_2 \cdot k + m_t^2\Gamma_t^2)}{\left[(q_1 \cdot k)^2 + m_t^2\Gamma_t^2\right]\left[(q_2 \cdot k)^2 + m_t^2\Gamma_t^2\right]} . \tag{10}$$

These functions have the (formal) property that $\chi_i, \chi_{12} \to 0$ as $\Gamma_t \to 0$, and $\chi_i, \chi_{12} \to 1$ as $\Gamma_t \to \infty$. In the former limit, we have

$$\begin{aligned} \mathcal{F} \to {} & \mathcal{F}_0 + c_7\left[\widehat{q_1q_1} + \widehat{p_1p_1} - 2\widehat{q_1p_1}\right] \\ & + c_8\left[\widehat{q_2q_2} + \widehat{p_2p_2} - 2\widehat{q_2p_2}\right] , \end{aligned} \tag{11}$$

which is the stable top result together with additional $\widehat{tb}$ and $\widehat{\bar{t}\bar{b}}$ antennae [4]. In the other extreme, $\chi_i, \chi_{12} \to 1$, the top quarks decay immediately after production and the radiation pattern is identical to that for the process

$$A(k_1) + B(k_2) \to b(p_1) + \bar{b}(p_2) \tag{12}$$

at reduced invariant squared energy $W^2 = (p_1 + p_2)^2$ in

TABLE I. The c_i coefficients of Eq. (6) for $t\bar{t}$ production, for SU(N) color with $C_F = (N^2-1)/(2N)$.

Process	c_1	c_2, c_5	c_3, c_4	c_6	c_7, c_8
$e^-e^+ \to t\bar{t}$	0	0	0	$2C_F$	$-C_F$
$q\bar{q} \to Z^* \to t\bar{t}$	$2C_F$	0	0	$2C_F$	$-C_F$
$gg \to H \to t\bar{t}$	$2N$	0	0	$2C_F$	$-C_F$
$q\bar{q} \to t\bar{t}$	$-\frac{1}{N}$	$2C_F - \frac{1}{N}$	$\frac{2}{N}$	$-\frac{1}{N}$	$-C_F$
$gg \to t\bar{t}$	$-2C_F + 2N + 2Y$	$C_F - X - Y$	$C_F + X - Y$	2Y	$-C_F$

the final state.

(ii) The functions X and Y appearing in the coefficients for the $gg \to t\bar{t}$ process are given by

$$X = \frac{N^2}{4C_F}\left[(1+2\mu)\left(\frac{1}{U}-\frac{1}{T}\right) -\mu^2\left(\frac{1}{U^2}-\frac{1}{T^2}\right)+2(U-T)\right] \times\left[\frac{1}{UT}-\frac{N}{C_F}\right]^{-1}\left[T^2+U^2+2\mu-\frac{\mu^2}{UT}\right]^{-1} \quad (13)$$

and

$$Y = \frac{1}{4C_F}\left[\frac{1}{N^2UT}+2\right]\left[\frac{1}{UT}-\frac{N}{C_F}\right]^{-1}, \quad (14)$$

where

$$T=\frac{k_1\cdot q_1}{k_1\cdot k_2}, \qquad U=\frac{k_1\cdot q_2}{k_1\cdot k_2}, \qquad \mu=\frac{m_t^2}{k_1\cdot k_2}. \quad (15)$$

(The X and Y functions here are closely related to those given in Ellis and Sexton [6]; here we have normalized X and Y by dividing them by the $gg \to t\bar{t}$ squared amplitude.) Figure 1 shows the functions X and Y plotted versus the t quark scattering angle (in the gg center-of-mass frame) for three different beam energies. Note that at threshold $T = U = \mu = 1/2$ and

$$X = 0, \qquad Y = \frac{1}{2N^2}\,\frac{2+N^2}{4C_F-N} = \frac{11}{42} \quad (N=3). \quad (16)$$

The numerically small values of Y [$Y/X \sim O(1/N^2)$], together with the fact that collinear singularities are absent from the corresponding combination of antennae, leads to a negligible contribution from this piece in practice [6,7]. The contributions from the $t\bar{t}$ antenna are not suppressed by $1/N^2$ in processes (3a), (3b), and (3c), where the $t\bar{t}$ pair is produced in a color singlet state. In processes (3d) and (3e), the azimuthal asymmetry of emission off t quarks is violated even in the large N limit, because of the presence of the $\widehat{k_iq_j}$ antennae.

(iii) Although the bulk of the coefficients in Table I are simply color factors, independent of the subprocess invariants, the cross section for soft gluon radiation does *not* in general factorize into an eikonal factor times the lowest-order cross section. This lack of factorization is the origin of the X and Y terms appearing in Table I for the $gg \to t\bar{t}$ process. The reason can be traced to the color structure of the $2 \to 2$ process [7,8]. For all but the $gg \to t\bar{t}$ process, the color flow at the amplitude level can be uniquely represented by continuous lines ("strings") linking the external particles. Thus Figs. 2(a) and (b) show the color flow for $e^-e^+ \to t\bar{t}$ and $q\bar{q} \to t\bar{t}$, respectively. Note that in the leading $1/N$ limit (the planar limit) there is a one-to-one correspondence between the color flow lines and the nonzero antenna coefficients. In contrast, the $gg \to t\bar{t}$ process has two possible color flows at the amplitude level as shown in Figs. 2(c) and (d). It is the interference between these two contributions that spoils the identification of the color flows in the planar limit. However, this interference is suppressed in the large N limit, where we find

$$\mathcal{F} \to \frac{1}{4}(N-2X)\left[2\widehat{k_1q_1}+2\widehat{k_2q_2}+2\widehat{k_1k_2}-\widehat{q_1q_1}-\widehat{q_2q_2}\right]+\frac{1}{4}(N+2X)\left[2\widehat{k_1q_2}+2\widehat{k_2q_1}+2\widehat{k_1k_2}-\widehat{q_1q_1}-\widehat{q_2q_2}\right], \quad (17)$$

which is the separation into two positive-definite color structures discussed in Ref. [7].

(iv) In the large N limit, the $\widehat{t\bar{b}}$ and $\widehat{\bar{t}b}$ antennae can interfere only in the case of the first three processes in Eq. (3). For processes 3d and 3e, in this limit, the decays are uncorrelated in color and the interference is absent.

III. NUMERICAL RESULTS

In the previous section we have seen how the different color structure of the various processes leads to different weightings of the antennae contributions. In this section we study the implications of this for the actual gluon

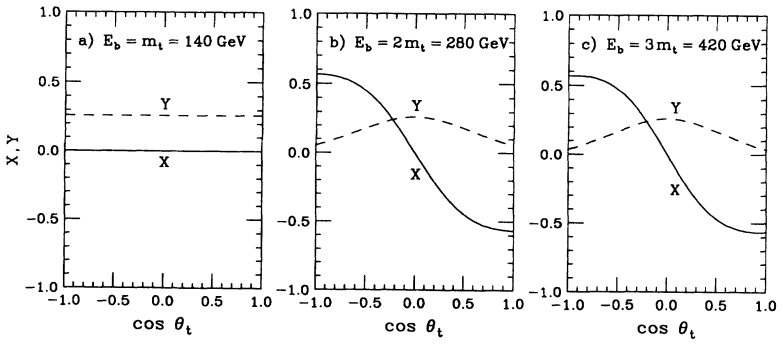

FIG. 1. Dependence of the nonfactorizing functions X (solid lines) and Y (dashed lines) for $gg \to t\bar{t}$ on the center-of-mass scattering angle of the t quark, for beam energies $E_{\text{beam}} = m_t$ (threshold), $2m_t$, and $3m_t$.

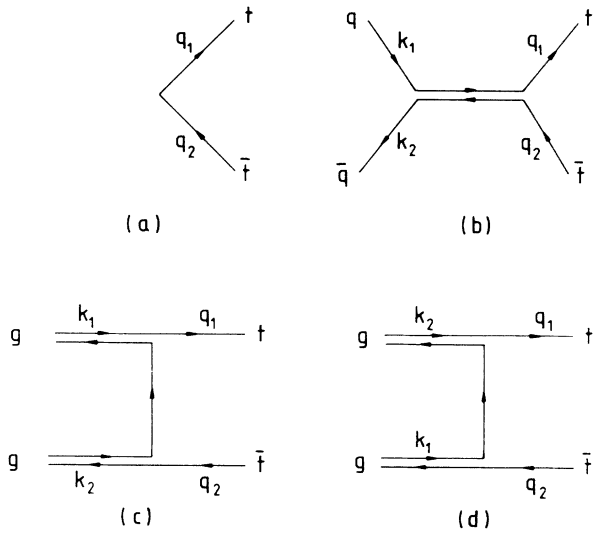

FIG. 2. Color flow diagrams for the processes (a) $e^+e^- \to t\bar{t}$, (b) $q\bar{q} \to t\bar{t}$, and (c),(d) $gg \to t\bar{t}$.

distribution. Our purpose is not to give a comprehensive treatment of all the possibilities, but rather to consider some simple configurations which illustrate the underlying physics.

In studying the way in which the various antennae contribute, it is instructive to consider all five processes listed in Eq. (3). Since we may neglect the soft gluon in the kinematics, the t and $\bar{t}$ momenta are back to back in the center-of-mass frame of the collision. The b- and $\bar{b}$-momenta are also taken to be back to back. This is for simplicity only—the qualitative features are unchanged as long as the $b\bar{b}$ angle is not chosen particularly small.

Distributions of the soft gluon radiation in the polar and azimuthal angles (relative to the beam direction) are presented for a soft gluon with energy $\omega_g = 5$ GeV. Again, this value is not critical: What matters as far as the interference contributions are concerned is the relative size of ω_g and Γ_t. Our results should be interpreted as referring to the distribution of a soft hadronic jet accompanying the significantly more energetic $bW^+\bar{b}W^-$ particles. The distributions are calculated at the parton level and are plotted in the parton subprocess center-of-mass frame. Unless otherwise stated, we assume a parton beam energy of $E_{\text{beam}} = 2m_t$, motivated by the fact that at hadron colliders the average subprocess center-of-mass energy is several times the threshold energy for $t\bar{t}$ production. A realistic study of soft gluon radiation in hadronic $t\bar{t}$ production would of course require a convolution of the parton-level cross sections with parton distribution functions. Such a convolution would smear the results illustrated here, although one could in principle reconstruct this frame directly if all the top quark decay products were measured.

The following shorthand notation will be used to denote the polar (θ_g) and azimuthal angle (ϕ_g) distributions:

$$\frac{dN}{d\cos\theta_g} \equiv \omega_g \frac{1}{d\sigma_0} \frac{d\sigma}{d\omega_g d\cos\theta_g d\phi_g}\bigg|_{\substack{\phi_g=0^\circ \\ \omega_g=5\ \text{GeV}}}$$

$$= \frac{\alpha_s}{4\pi^2}\omega_g^2 \mathcal{F}(\theta_g) \tag{18}$$

and

$$\frac{dN}{d\phi_g} \equiv \omega_g \frac{1}{d\sigma_0} \frac{d\sigma}{d\omega_g d\cos\theta_g d\phi_g}\bigg|_{\substack{\theta_g=90^\circ \\ \omega_g=5\ \text{GeV}}}$$

$$= \frac{\alpha_s}{4\pi^2}\omega_g^2 \mathcal{F}(\phi_g)\,. \tag{19}$$

Recall that in the soft gluon approximation, the gluon energy distribution falls as $1/\omega_g$. Thus an extra factor of ω_g has been included in the above definitions to make the distributions dimensionless quantities. The numerical results presented here have been generated using the following input parameters: $m_t = 140$ GeV, $m_b = 5$ GeV, $M_W = 80$ GeV, and $\alpha_s = 0.1$. For all the distributions, the coordinate system is chosen such that the three-momenta of the incoming partons are along

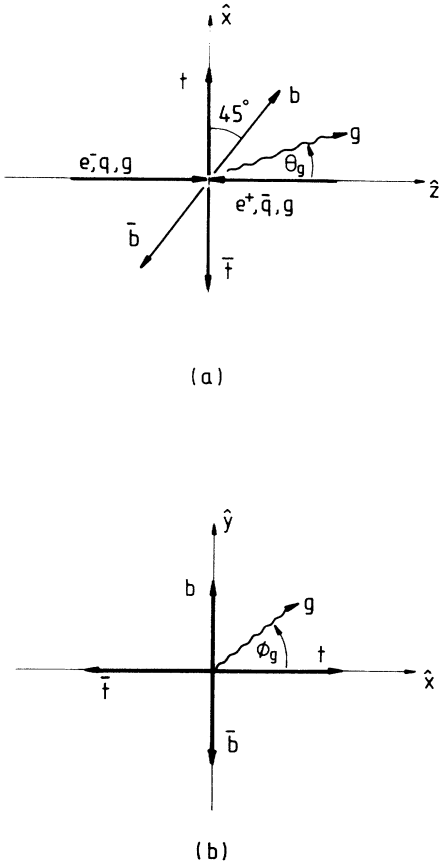

FIG. 3. (a) The orientation of the three-momentum vectors for the $dN/d\cos\theta_g$ distributions. All three-momentum vectors are chosen to lie in the xz plane. The $\hat{y}$ axis is perpendicular to the page. (b) The orientation of the three-momentum vectors for the $dN/d\phi_g$ distributions. The three-momentum vectors of the outgoing partons are chosen to lie in the xy plane. The three-momentum vectors of the incoming partons are along the $\hat{z}$ axis which is perpendicular to the page.

the $\pm\hat{z}$ directions. Furthermore, the three-momenta of the outgoing t and $\bar{t}$ are chosen to be in the $+\hat{x}$ and $-\hat{x}$ directions, respectively. For the $dN/d\cos\theta_g$ distributions, the three-momenta of the b and $\bar{b}$ quarks are chosen to be back to back in the xz plane, with the b-quark three-momentum vector 45° away from the t-quark three-momentum vector as illustrated in Fig. 3(a). The soft gluon three-momentum is also taken to be in the xz plane, and thus the three-momenta of all the partons lie in the xz plane as depicted in Fig. 3(a). For the $dN/d\phi_g$ distributions, the three-momenta of all the final state partons are taken to be in the xy plane, which is transverse to the momenta of the incoming partons; see Fig. 3(b).

We begin by presenting results for the polar angle distribution of the soft gluon. Figure 4 shows $dN/d\cos\theta_g$ versus θ_g for incoming partons with energy $E_{\rm beam} = 2m_t = 280$ GeV, where $m_t = 140$ GeV is the top quark mass. The standard model Born value $\Gamma_t = \Gamma^{(0)}_{\rm SM} = 0.67$ GeV for $m_t = 140$ GeV has been used for the top quark width. The soft gluon radiation patterns for the five processes listed in Eq. (3) are shown in the figure. The angles of the incoming and outgoing partons are indicated at the top of the figure. The divergence in the radiation pattern at $\theta_g = 0°$ and 180° (and 360°) for the hadronic production processes is the initial state collinear singularity, i.e., $q \to q+g$, $g \to g+g$. The strength of the singularity simply reflects the color charge of the incoming particles. For example, the radiation pattern in the region $\theta_g \approx 0°$ is dominated by the antennae containing a factor of k_1. If k is almost parallel to k_1, then

$$\widehat{k_1 a} \approx \frac{2}{\omega_g^2}\,\frac{1}{\theta_g^2}\,, \tag{20}$$

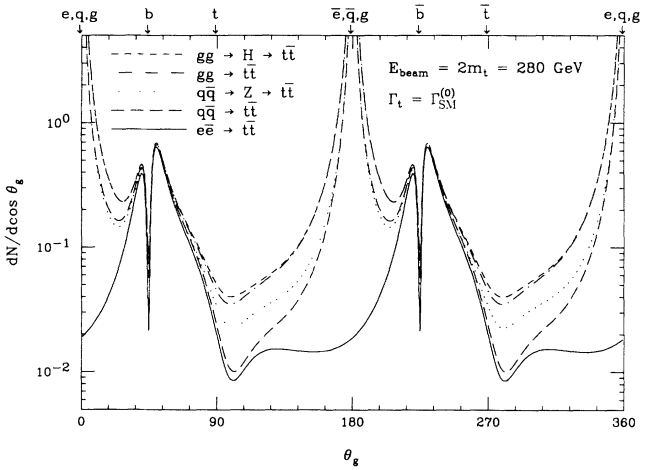

FIG. 4. Distribution of the soft gluon radiation in the polar angle θ_g; $dN/d\cos\theta_g$ is plotted versus θ_g for a soft gluon with energy $\omega_g = 5$ GeV. Curves are shown for the five processes listed in Eq. (3). The energy of the incoming partons is $E_{\rm beam} = 2m_t = 280$ GeV, where $m_t = 140$ GeV is the top quark mass. The standard model Born value has been used for the top quark width. The directions of the incoming and outgoing partons are indicated at the top of the figure. The energies and angles are measured in the parton center-of-mass frame.

independent of the other momentum (a^μ) in the antenna. There are three such terms on the right-hand-side of Eq. (6), and hence

$$\mathcal{F} \approx \frac{2}{\omega_g^2}\,\frac{c_1+c_2+c_3}{\theta_g^2}\,. \tag{21}$$

From Table I, we see that $c_1 + c_2 + c_3 = 2C_F$ ($2N$) for the $q\bar{q}$ (gg) initiated processes, respectively. Thus near $\theta_g = 0°$ and 180° the curves for the gg initiated processes are larger than those for the $q\bar{q}$ initiated processes, while the nonsingular e^-e^+ distribution is very small.

In the same way, all of the processes exhibit a sharp dip in the radiation pattern in the direction of the b and $\bar{b}$ quarks when $m_b/E_b \ll 1$. These dips are the well known heavy-quark dead cones [10]. For example, close to the b-quark direction we have [cf., Eq. (20)]

$$\widehat{p_1 a} \approx \frac{2}{\omega_g^2}\,\frac{\tilde{\theta}_g^2}{\left[\tilde{\theta}_g^2 + (m_b/E_b)^2\right]^2}\,, \tag{22}$$

where now $\tilde{\theta}_g$ is the angle between the gluon and b-quark directions. The angular width of these dead cones is proportional to m_b/E_b. Again, it is straightforward to check that the dead-cone behavior near the b-quark directions is the same for all processes. This follows from the fact that $c_2 + c_4 + c_6 = -2c_7 = 2C_F$ (see Table I).

The corresponding dead cones about the t and $\bar{t}$ quark directions are much broader due to the larger top quark mass. The minimum of the $t(\bar{t})$ quark dead cone does not coincide with the t ($\bar{t}$) quark direction; instead, the minimum is shifted to a slightly larger angle. This is because the $\widehat{q_1 p_1}$ and $\widehat{q_2 p_2}$ terms in Eq. (8) give a contribution which is a decreasing function of θ_g in the neighborhood around the t ($\bar{t}$) quark direction, whereas the contribution from the other terms has a minimum in the t ($\bar{t}$) quark direction. The resulting sum thus has a minimum at a value of θ_g that is slightly larger than the direction of the t ($\bar{t}$) quark. The other interesting feature to note in Fig. 4 is the difference between the distributions for the $q\bar{q} \to Z^* \to t\bar{t}$ and $q\bar{q} \to t\bar{t}$ processes. The presence of the $\widehat{k_1 q_1}$ and $\widehat{k_2 q_2}$ antenna for the latter *increases* the radiation between the q and b quarks, and *decreases* that between the b and $\bar{q}$ quarks, relative to the former process. The effect is clearly seen in the dips on either side of the b-quark dead cone in Fig. 4.

Figure 5 shows $dN/d\cos\theta_g$ versus θ_g for incoming partons with energy $E_{\rm beam} = 2m_t = 280$ GeV as in Fig. 4, but now with the top quark width taken to the formal limit $\Gamma_t \to \infty$. In this limit, the interference factors χ_1, χ_2, and χ_{12} in Eqs. (9) and (10) all go to 1. This limit corresponds to the top quark decaying instantly; thus the resulting radiation pattern is equivalent to the radiation pattern for $b\bar{b}$ production. In particular, the radiation pattern is independent of the t ($\bar{t}$) direction. Comparing the case of $\Gamma_t = \Gamma^{(0)}_{\rm SM}$ in Fig. 4 with the present case of $\Gamma_t = \infty$, we see that with the exception of the e^-e^+ process, the radiation is again not symmetric around the b ($\bar{b}$) dead cone. However, the maximum now appears on the side of the cone closest to the incoming beam di-

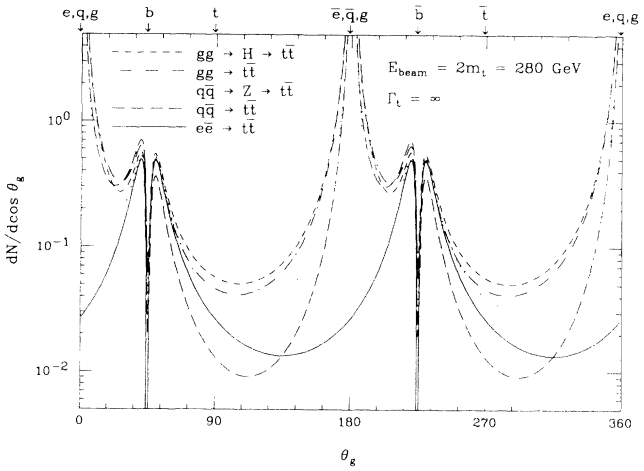

FIG. 5. Same as Fig. 4 but now the top quark width has been set to $\Gamma_t = \infty$, which is equivalent to $b\bar{b}$ production.

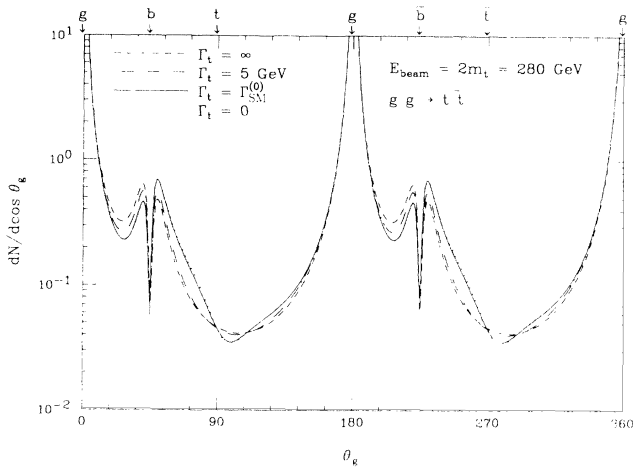

FIG. 6. $dN/d\cos\theta_g$ versus θ_g for the process $gg \to t\bar{t}$ for four values of the top quark width: $\Gamma_t = \infty$, 5 GeV, 0.67 GeV (standard model Born value), and 0. The energy of the soft gluon is $\omega_g = 5$ GeV and the energy of the incoming gluons is $E_{\rm beam} = 2m_t = 280$ GeV. The directions of the incoming and outgoing partons are indicated at the top of the figure. The energies and angles are measured in the parton center-of-mass frame.

rection. For the reasons noted above, the asymmetry is particularly strong for the $q\bar{q} \to t\bar{t}$ process. We also see that in the regions where the t ($\bar{t}$) dead cones were previously located ($\theta_g \approx 100°$ and 280°), the $e^-e^+ \to t\bar{t}$ and $q\bar{q} \to t\bar{t}$ curves have changed considerably, whereas the $gg \to H \to t\bar{t}$ and $gg \to t\bar{t}$ curves have changed little. For these latter processes, the radiation pattern receives a larger contribution from radiation off the initial state gg, which is of course independent of Γ_t. On the other hand, the radiation patterns for the $e^-e^+ \to t\bar{t}$ and $q\bar{q} \to t\bar{t}$ processes are more sensitive to the radiation from the final state quarks, which is very different for the two cases of $b\bar{b}$ production versus $t\bar{t}$ production and decay.

The variation of the radiation pattern with the top quark width is illustrated in Fig. 6 for the process $gg \to t\bar{t}$. As before, the distribution $dN/d\cos\theta_g$ is plotted versus θ_g for incoming partons with energy $E_{\rm beam} = 2m_t = 280$ GeV. Curves are shown for four values of the top quark, width: $\Gamma_t = \infty$, 5 GeV, 0.67 GeV (the standard model Born value), and 0. The radiation pattern for the standard model Born top quark width is very close to the radiation pattern for $\Gamma_t = 0$. Between the incoming $g(k_1)$ and the b quark, the $\widehat{k_1 p_1}$ antenna causes the radiation to increase as Γ_t (and hence χ_1) increases. On the other side of the b-quark dead cone, the effect of emission from the top quark is seen to decrease as Γ_t increases. On the whole, however, the curves show that the $gg \to t\bar{t}$ process is not very sensitive to the top quark width. The $q\bar{q} \to t\bar{t}$ process on the other hand is much more sensitive to the top quark width (see Figs. 4 and 5).

A more graphic representation of the effects described above can be obtained by considering the radiation pattern in polar coordinates. Thus Fig. 7 shows $dN/d\cos\theta_g$ versus θ_g, with the distance from the origin proportional to the magnitude of the distribution. As before, all particles lie in the xz plane; their directions are indicated by arrows on the figure. The radiation pattern for the process $gg \to t\bar{t}$ is shown for two values of the top quark width: the standard model Born value and the $\Gamma_t \to \infty$ limit which is equivalent to $b\bar{b}$ production. (Note that this is simply a different representation of the same two curves in the previous figure.) The collinear singularities along the $\pm\hat{z}$ directions are clearly evident, as are the dead cones about the b ($\bar{b}$) and t ($\bar{t}$) quark directions. Notice again that the asymmetry of the lobes about the b-quark direction is different for the two cases, for the reasons discussed earlier.

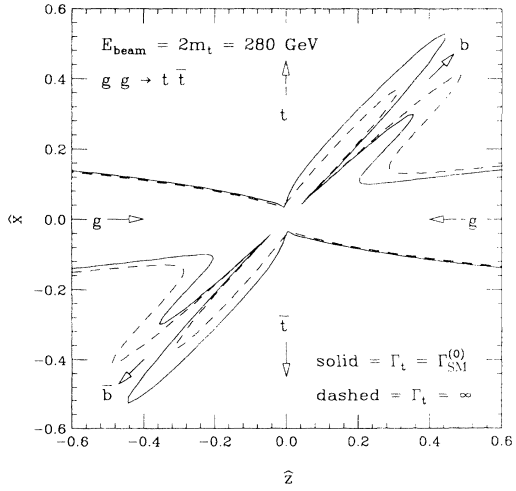

FIG. 7. $dN/d\cos\theta_g$ versus θ_g plotted in polar coordinates. The radiation pattern for the process $gg \to t\bar{t}$ is illustrated for $\Gamma_t = \Gamma_{\rm SM}^{(0)}$ (solid line) and $\Gamma_t = \infty$ (dashed line). The energy of the soft gluon is $\omega_g = 5$ GeV and the energy of the incoming gluons is $E_{\rm beam} = 2m_t = 280$ GeV. The directions of the incoming and outgoing partons are indicated at the top of the figure. The energies and angles are measured in the parton center-of-mass frame.

The polar angle distributions presented above emphasize the contributions involving radiation from the incoming particles, i.e., the antennae involving k_1 and k_2. To focus on the radiation from the final state particles it is useful to consider the azimuthal angle distribution of the soft gluon radiation. The three-momenta of the final state partons are now fixed to lie in the plane transverse to the incoming partons. In this configuration, the effects of the initial state radiation are minimized. We might therefore expect the $dN/d\phi_g$ distributions to be more similar than the $dN/d\cos\theta_g$ distributions for the five processes listed in Eq. (3). Figure 8 shows the azimuthal distribution of soft gluon radiation when all the outgoing partons are in the transverse plane. Distributions are again shown for the five processes listed in Eq. (3). The directions of the three-momenta of the outgoing heavy quarks are indicated at the top of the figure. The momenta of the t and $\bar{t}$ quarks are at 0° and 180°, respectively, while the b and $\bar{b}$ momenta are at 90° and 270°, respectively. The dead cones in the directions of the t and b ($\bar{t}$ and $\bar{b}$) quarks are clearly evident in this figure. The width of the dead cones is proportional to m_Q/E_Q, and thus the t ($\bar{t}$) quark dead cone is much wider than the b ($\bar{b}$) quark dead cone. The minimum in the t ($\bar{t}$) dead cone does not coincide with the t ($\bar{t}$) direction; instead, the minimum is shifted to a slightly smaller angle. The reason for this shift is the same as discussed for the $dN/d\cos\theta_g$ distribution in Fig. 4, except that now the $\widehat{q_1p_1}$ and $\widehat{q_2p_2}$ terms in Eq. (8) give a contribution which is an increasing function of ϕ_g in the neighborhood around the direction of the t ($\bar{t}$) quark. The contribution from the other terms has a minimum in the t ($\bar{t}$) direction and is symmetric about this direction. The resulting sum now has a minimum at a value of ϕ_g

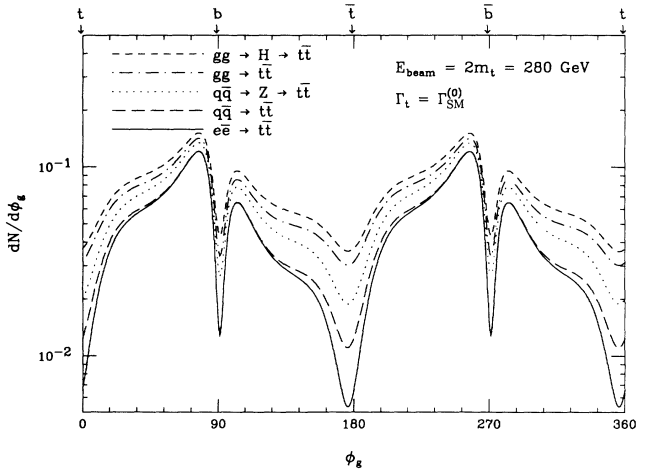

FIG. 8. Distribution of the soft gluon radiation in the azimuthal angle ϕ_g; $dN/d\cos\phi_g$ is plotted versus ϕ_g for a soft gluon with energy $\omega_g = 5$ GeV. Curves are shown for the five processes listed in Eq. (3). The energy of the incoming partons is $E_{\rm beam} = 2m_t = 280$ GeV, where $m_t = 140$ GeV is the top quark mass. The standard model Born value has been used for the top quark width. The directions of the incoming and outgoing partons are indicated at the top of the figure. The b ($\bar{b}$) quark is 90° away from the t ($\bar{t}$) quark. The energies and angles are measured in the parton center-of-mass frame.

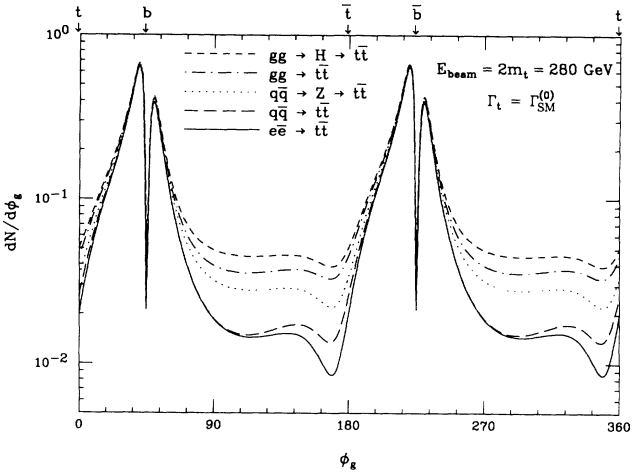

FIG. 9. Same as Fig. 8 but now the b ($\bar{b}$) quark is 45° away from the t ($\bar{t}$) quark.

that is slightly smaller than the t ($\bar{t}$) quark direction. The $\widehat{t\bar{b}}$ antennae, i.e., the $\widehat{q_1p_1}$ and $\widehat{q_2p_2}$ terms in Eq. (8), are also responsible for the lack of symmetry in the radiation pattern about the t and b quark directions. Note that the ordering of the different processes is preserved over the complete ϕ_g range, with the effects of the initial radiation providing an approximately constant background to the dominant contributions involving the t and b quarks. The ordering reflects the color charges of the initial particles, $gg > q\bar{q} > e^-e^+$. Note, however, that the hadronic production processes are suppressed relative to the corresponding s-channel color singlet-processes, e.g., $(q\bar{q} \to Z^* \to t\bar{t}) > (q\bar{q} \to t\bar{t})$. The reason, evident in Table I, is the suppression of the $\widehat{t\bar{t}}$ antenna (the coefficient c_6) for the hadronic production processes.

Figure 9 is the same as Fig. 8, except that now the b and $\bar{b}$ momenta have been fixed at 45° and 235°, respectively. The b ($\bar{b}$) quark is now closer to the t ($\bar{t}$) direction, consequently, the b ($\bar{b}$) quark is now moving faster, and thus the b ($\bar{b}$) quark dead cone is now narrower than

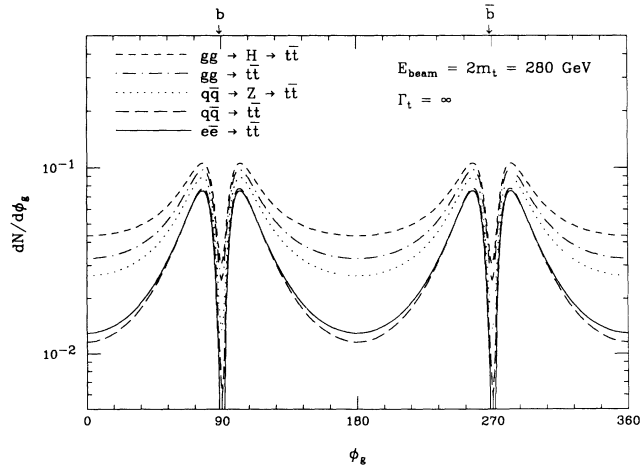

FIG. 10. Same as Fig. 8 but now the top quark width has been set to $\Gamma_t = \infty$, which is equivalent to $b\bar{b}$ production.

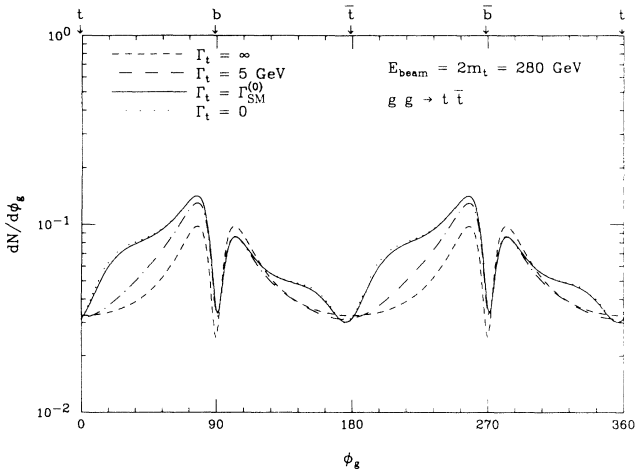

FIG. 11. $dN/d\phi_g$ versus ϕ_g for the process $qq \to t\bar{t}$ for four values of the top quark width: $\Gamma_t = \infty, 5$ GeV, 0.67 GeV (standard model Born value), and 0. The energy of the soft gluon is $\omega_g = 5$ GeV and the energy of the incoming gluons is $E_{\rm beam} = 2m_t = 280$ GeV. The directions of the outgoing partons are indicated at the top of the figure. The energies and angles are measured in the parton center-of-mass frame.

in the previous figure. If the trend of moving the b ($\bar{b}$) quark closer to the t ($\bar{t}$) quark direction continues, the b ($\bar{b}$) quark continues to move faster and its dead cone continues to narrow. In the limiting case of the t and b ($\bar{t}$ and $\bar{b}$) quarks parallel, the dead cone is very narrow and the radiation pattern is symmetric about the $t\,b$ and $\bar{t}\,\bar{b}$ directions.

Figure 10 is the same as Fig. 8, but with the top quark width set to infinity. This corresponds to the top quark decaying instantly, and so the radiation pattern is equivalent to that of $b\bar{b}$ production. The major difference between this figure and Fig. 8 is the lack of the top quark dead cones in the present figure. The radiation pattern is now symmetric about the b and $\bar{b}$ directions. (The t and $\bar{t}$ directions are irrelevant since the t and $\bar{t}$ decay instantly). Notice that the magnitude of the $q\bar{q} \to t\bar{t}$ curve is now less than the $e^-e^+ \to t\bar{t}$ curve. The reason for this is that in the limit $\Gamma_t \to \infty$ ($\chi_{12} \to 1$) the $\widehat{p_1p_2}$ antenna (negative) contribution is enhanced. The color suppression of this contribution in the $q\bar{q} \to t\bar{t}$ case is no longer compensated by the background initial state radiation.

The variation of the azimuthal radiation pattern with the top quark width is illustrated in Fig. 11 for the process $gg \to t\bar{t}$. The distribution $dN/d\phi_g$ is plotted versus ϕ_g for incoming partons with energy $E_{\rm beam} = 2m_t = 280$ GeV. The radiation pattern is shown for four values of the top quark width: $\Gamma_t = \infty$, 5 GeV, 0.67 GeV (the standard model Born value), and 0. The radiation pattern for the standard model Born top quark width is almost identical to the $\Gamma_t = 0$ pattern. The dead cone about the $t\,(\bar{t})$ quark is obscured already for $\Gamma_t = 5$ GeV.

In Fig. 12 we plot $dN/d\phi_g$ versus ϕ_g in polar coordinates. The radiation pattern for the process $gg \to t\bar{t}$ is shown for $\Gamma_t = \Gamma_{\rm SM}^{(0)}$ (solid line) and $\Gamma_t = \infty$ (dashed line). The angle between the momenta vectors of the t and b quarks is 0°, 45°, 90°, 135°, and 180°, for parts (a), (b), (c), (d), and (e), respectively. The radiation patterns are quite different for the two cases. The $b\bar{b}$ radiation pattern (dashed line) is always symmetric about the $b\bar{b}$ direction. (The $t\bar{t}$ direction is irrelevant in this case.) For the standard model width (solid line), the radiation is always largest in the angular sector between the t and b ($\bar{t}$ and $\bar{b}$) directions. For example, in part (c), the radiation in the first and third quadrants is much larger than in the second or fourth quadrants. This is a consequence of the color antenna connecting the t and b ($\bar{t}$ and $\bar{b}$) quarks. As the angle between the t and b quarks increases, the velocity of the b quark decreases, the b quark dead cone becomes wider, the magnitude of the radiation decreases, and the radiation pattern becomes more isotropic.

IV. SUMMARY

In this paper we have calculated the soft gluon distribution in $t\bar{t}$ production, taking the decay of the top

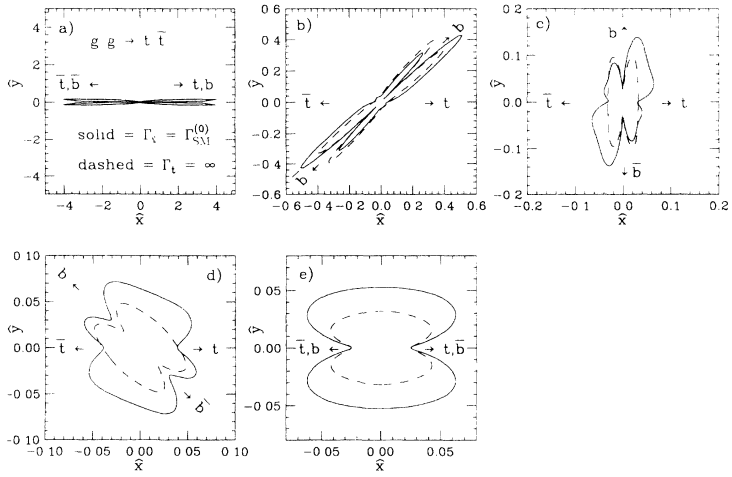

FIG. 12. $dN/d\phi_g$ versus ϕ_g plotted in polar coordinates. The radiation pattern for the process $gg \to t\bar{t}$ is illustrated for $\Gamma_t = \Gamma_{\rm SM}^{(0)}$ (solid line) and $\Gamma_t = \infty$ (dashed line). The energy of the soft gluon is $\omega_g = 5$ GeV and the energy of the incoming gluons is $E_{\rm beam} = 2m_t = 280$ GeV. The angle between the $t\,(\bar{t})$ and $b\,(\bar{b})$ quarks is $0°, 45°, 90°, 135°$, and 180° in parts (a), (b), (c), (d), and (e), respectively. The directions of the outgoing partons are indicated by arrows on the figure. The energies and angles are measured in the parton center-of-mass frame.

quarks fully into account. Although our primary interest is in hadronic $t\bar{t}$ production, we have also considered several other processes with different color structures. This allows us to quantify the contributions from the different antennae which determine the radiation patterns.

We have seen how, in general, the radiation pattern depends on the color flow in the $2 \to 2$ process, the orientation of the final state particles with respect to the beam and to each other, and on the top decay width. The latter controls the interference between radiation before and after the top decay and between radiation in two decays. When the decay width is large, the b and $\bar{b}$ appear almost instantaneously and they can radiate coherently, as though produced directly.

We have focused in particular on two types of distributions. The distribution in polar angle of the gluon with respect to the beam is sensitive to radiation off the initial state particles, and also to the presence of antennae linking the initial and final state particles (which are absent in s-channel color-singlet exchange processes). When all the final state particles are in the transverse plane, the distribution in the gluon azimuthal angle is more sensitive to the radiation off the final state particles, in particular to the dead cones of the t and b quarks.

The study of soft gluon radiation in $t\bar{t}$ events is important not only for theoretical reasons. The effects we have calculated are responsible for the distribution of soft hadrons and jets accompanying the final state b's and W's. These in turn could play an important role in the determination of the top mass from the reconstructed invariant mass of its decay products. For example, the interference between emission *before* and *after* top decay constitutes an irreducible uncertainty in such a procedure. It is important that Monte Carlo routines used to correct for these effects in the data contain all the relevant underlying physics.

ACKNOWLEDGMENTS

This work was supported in part by the U.K. Science and Engineering Research Council. We are grateful to Yuri Dokshitzer and Lynne Orr for useful discussions.

[1] P. Langacker, University of Pennsylvania Report No. UPR-0555-T, 1993 (unpublished).
[2] CDF Collaboration, A. Caner, in XXVIIth Recontres de Moriond, 1993 (unpublished).
[3] D0 Collaboration, M. Narain, in XXVIIth Recontres de Moriond, 1993 (unpublished).
[4] V. A. Khoze, L. H. Orr, and W. J. Stirling, Nucl. Phys. **B378**, 413 (1992); Yu. L. Dokshitzer, V. A. Khoze, L. H. Orr, and W. J. Stirling, *ibid.* **B403**, 65 (1993).
[5] G. Jikia, Phys. Lett. B **257**, 196 (1991) .
[6] R. K. Ellis and J. C. Sexton, Nucl. Phys. **B282**, 642 (1987) .
[7] G. Marchesini and B. R. Webber, Nucl. Phys. **B330**, 261 (1990) .
[8] Yu. L. Dokshitzer, V. A. Khoze, A. H. Mueller, and S. I. Troyan, *Basics of Perturbative QCD* (Editions Frontières, Gif-sur-Yvette, France, 1991).
[9] L. H. Orr, Phys. Rev. D **44**, 88 (1991).
[10] Yu. L. Dokshitzer, V. A. Khoze, and S. I. Troyan, J. Phys. G **17**, 1481 (1991); **17**, 1602 (1991).